

The transition to strong convection

J. DAVID NEELIN,* OLE PETERS AND KATRINA HALES

Dept. of Atmospheric and Oceanic Sciences and Institute of Geophysics and Planetary Physics,

University of California, Los Angeles

Submitted to *J. Atmos. Sci.* Sept. 25, 2008

ABSTRACT

Recent work has shown that observations of tropical precipitation conform to properties associated with critical phenomena in other systems. Here some of these universal properties are used to probe the physics of tropical convection empirically, providing potential tests for models and parameterizations. The power law pickup of ensemble average precipitation as a function of column water vapor w occurs above a critical value w_c whose temperature dependence is determined for layer-integrated tropospheric temperature or saturation value. This dependence differs from the simplest expectations based on column saturation. Rescaling w by w_c permits a collapse of precipitation-related statistics to similar functional dependence for all temperatures. The sharp precipitation variance peak at w_c , obtained without detailed vertical structure information, appears consistent with arguments that onset requires a deep moist layer. Sea surface temperature (SST) is found *not* to have significant effect on the precipitation pickup. The effect of SST on the climatological precipitation occurs via the frequency of occurrence of w values as the system spends a larger fraction of time near criticality over regions of warm SST. Near and above criticality, where most precipitation occurs, the w -distribution is highly constrained by the interaction with convection, with a characteristic sharp drop at criticality. For precipitating points, the distribution has a Gaussian core with exponential tail akin to forced advection-diffusion problems. The long tail above w_c , implying relatively frequent strong events, remains similar through the range of tropospheric temperature and SST spanning tropical large-scale conditions. A simple empirical closure illustrates time decay properties.

1. Introduction

Convective parameterizations attempt to represent the dependence of the statistics of moist convection on water vapor and temperature. A reigning paradigm has been convective quasi-equilibrium (QE), in which buoyancy is assumed to be dissipated quickly at the convective scale. This forms the basis of many convective parameterizations (Manabe et al. 1965; Arakawa and Schubert 1974; Randall and Pan 1993; Zhang and McFarlane 1995; Pan and Randall 1998; Moorthi and Suarez 1992; Randall et al. 2003; Arakawa 2004; Zhang and Wang 2006). The simplifying implications of convective QE have also been the basis of much tropical dynamical theory for the interaction of convective scales with the large scale (e.g. Emanuel et al. 1994; Neelin and Zeng 2000; Bretherton and Sobel 2002). The combination of closure assumptions—the rate of reduction of buoyancy, the form of the assumed plumes, the entrainment properties—yields an increase in convective heating as moisture increases for a given temperature.

In one of the simplest examples, precipitation in the Betts and Miller (1986) scheme can be written, vertically integrating the expression for the moisture sink, as inte-

grating the expression for the moisture sink, as

$$P = \mathcal{H}(w - w_c(T)) (w - w_c(T)) / \tau_c, \quad (1)$$

where w is the column water vapor, i.e., the vertically integrated specific humidity, w_c is a threshold value at which precipitation is assumed to begin, and \mathcal{H} is the Heaviside function. The threshold w_c depends on the temperature through the convecting layer in a manner that is effectively parameterized as a given fraction of the saturation value, here vertically integrating over the pressure dependence. The precipitation is assumed to increase linearly, with a slope given by the assumed convective timescale, τ_c , say 2 hours. This example illustrates that the properties of the onset of convection with increasing moisture involve substantial assumptions (in this case including the time scale, the linear increase, and subsaturation value) that have not been well tested against observations, despite prior attempts to constrain QE (Xu and Randall 1998; Xu and Emanuel 1989).

Many studies indicate that representations of convection in climate and weather models have deficiencies and that the simulations are sensitive to this (e.g., Maloney and Hartmann 2001; Joseph and Nigam 2006; Biasutti et al.

2006; Dai 2006; Tost et al. 2006; Bretherton 2007), including to processes affecting the time dependence of adjustment by convection (Gregory and Rowntree 1990; Emanuel 1991, 1993; Pan and Randall 1998; Moorthi and Suarez 1992; Tompkins and Craig 1998); and to entrainment of moisture in the lower free troposphere (Derbyshire et al. 2004; Bechtold et al. 2008; Neale et al. 2008). The importance of moisture through the lower troposphere is supported by a growing body of observational evidence (Austin 1948; Yoneyama and Fujitani 1995; Wei et al. 1998; Raymond et al. 1998; Sherwood 1999; Parsons et al. 2000; Raymond 2000; Tompkins 2001; Redelsperger et al. 2002; Sobel et al. 2004; Tian et al. 2006). While this implies another significant dependence to be constrained, a fortunate consequence is that column water vapor, for which large data sets exist, is a good proxy (Holloway and Neelin 2008) for the onset of deep convective instability of entraining plumes. Together with the problem of constraining the statistics of short timescale convective processes for stochastic convective schemes (Buizza et al. 1999; Lin and Neelin 2000, 2003; Craig and Cohen 2006; Plant and Craig 2008; Tompkins and Berner 2008), these results point to a clear need to better characterize the transition to strong deep convection.

Bretherton et al. (2004) performed an analysis that motivated our own recent work, fitting empirically the increase of precipitation with column water vapor, corresponding to (1), with satellite microwave data on daily and monthly timescales. Examining the transition to strong convection at high time resolution, (Peters and Neelin 2006, PN hereafter) noted that the statistics conform to a number of properties of a continuous phase transition and the associated critical phenomena. This includes such properties as power law scaling of the precipitation variance with averaging scale. The pickup in precipitation above a critical value, instead of having the simple linear relation assumed in (1), approaches the power law expected from critical phenomena for the ensemble average conditioned on w :

$$\langle P \rangle = a[(w - w_c)/w_c]^\beta, \quad \text{if } (w - w_c) > 0, \quad (2)$$

Showing that the tropical convection conforms to some of the universal properties of continuous phase transitions is of interest because it organizes seemingly disconnected properties into a familiar bundle, and provides analogies to other systems that can suggest properties to investigate and methods by which to analyze them. Because some of these properties are universal, one might wonder whether specific information about tropical convection itself can be provided. Here, these properties are used to probe the physics of convection empirically, analyzing the transition in a thermodynamic plane that includes both column water vapor and tropospheric temperature. Initial results in this direction from Western Pacific data were used in combination with other observational constraints (Neelin et al.

2008) to postulate directions in which stochastic convection schemes might improve upon QE assumptions.

This study presents a multi-basin analysis in satellite microwave data of statistics relating to the continuous phase transition as a function of column water vapor and temperature, comparing various vertically integrated measures of temperature. A key ingredient is the empirical determination of the critical column water vapor as a function of temperature (section 3), which permits these statistics to be collapsed to very similar dependences for different temperatures. This then permits new features of the water vapor probability density function to be seen, including a sharp drop across the critical region, and an exponential tail above the critical point (section 4). These features are discussed in terms of prototypes from forced advection-diffusion problems and self-organized criticality. The high quality of the collapse when temperature dependence is included also enables discussion of the behavior below the critical point. Section 5 examines sea surface temperature (SST) dependence as an example of effects of large-scale forcing on these statistics. Implications for time dependence when the empirical ensemble mean precipitation relation is used for parameterization are then examined in section 6. The discussion includes potential practical applications, including for model evaluation.

2. Data

We use precipitation and column water vapor retrievals from the Tropical Rainfall Measuring Mission (TRMM; Kummerow et al. 2000), specifically the TRMM Microwave Imager (TMI) processed by Remote Sensing Systems (RSS) with the improved Hilburn and Wentz (2008) algorithm (version 4 TMI; also known as UMORA) that updates Wentz and Spencer (1998). We note the caveat that the microwave retrieval uses an empirical relation of precipitation to cloud water; a concurrent radar study will be noted in the text.

For tropospheric temperature data, the European Center for Medium Range Weather Forecasting (ECMWF) reanalysis (ERA40; Uppala and coauthors 2005) is used. While there are many reasons for caution in using certain variables from the reanalysis data set (Trenberth and Olsen 1988; Yu et al. 1998), the assimilation of microwave sounder unit temperature retrievals lends confidence to aspects with deep vertical structure consistent with the retrieval sensitivity (Spencer and Christy 1992). The beginning and end dates of the TMI and ERA40, respectively, determine our analysis period January 1998 through August 2002. The ERA40 temperatures are 6 hourly data on a 2.5 by 2.5 degree grid. For each TMI observation point, the temperatures from the ERA40 grid box containing it, and at the nearest time are used.

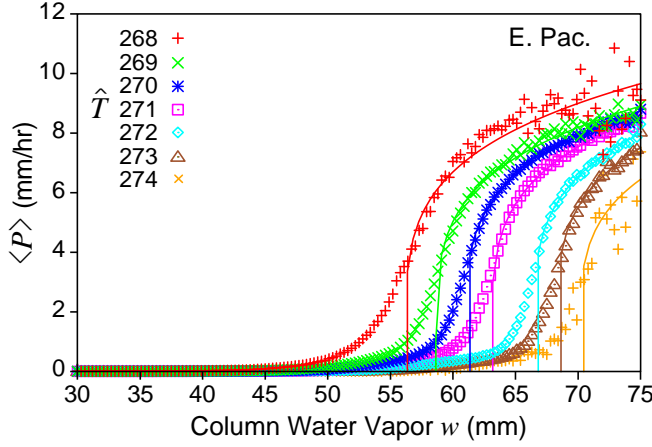


FIG. 1. Pickup of ensemble average precipitation $\langle P \rangle$, conditionally averaged by 0.3 mm bins of column water vapor w for 1K bins of the vertically averaged tropospheric temperature \hat{T} , for the eastern Pacific. Lines show power law fits above the critical point of the form (2).

3. Dependence of the deep convection transition on tropospheric temperature

To investigate the effect of tropospheric temperature on the transition to strongly precipitating deep convection, we need a simple measure of the tropospheric temperature that characterizes the leading variance and is reasonably well observed. We examine three simple measures: (i) vertically averaged tropospheric temperature \hat{T} (from 200 to 1000 hPa), for which we present most results; (ii) vertically integrated saturation value, $\widehat{q_{\text{sat}}}$, from 200 hPa to the surface pressure; (iii) saturation value integrated through a lower tropospheric layer (550–850 hPa), $\widehat{q_{\text{sat}}}^{LT}$. The latter two measures are further discussed in subsections 3b and 3c. In each case, the averages are in pressure coordinates, i.e., mass weighted.

Reasons for using \hat{T} include: the leading vertical structure of temperature variance tends to be coherent through the troposphere in the tropics, with temperature at each level correlating highly with tropospheric average (Holloway and Neelin 2007). Furthermore, microwave retrievals of tropospheric temperature tend to have an influence function through a deep layer (Christy et al. 2000) and these are assimilated in reanalysis data sets. This suggests that deep measures of tropospheric temperature are likely to be reasonably reliable even from the reanalysis data sets. This is aided by the long spatial correlation scale of temperature in the horizontal in the tropics. Detailed aspects of reanalysis vertical structure might not be reliable for present purposes (e.g., Trenberth and Guillemot 1998, and our own checks of reanalysis boundary layer variables against buoy data). Finally, for simple theoretical considerations, vertically integrated temperature provides a counterpart to the

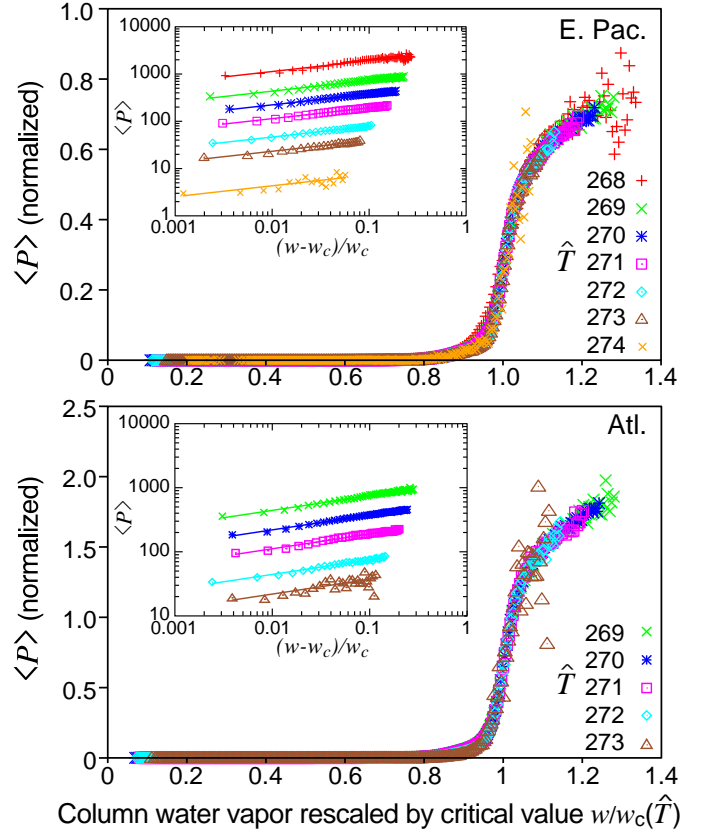


FIG. 2. a) Eastern Pacific ensemble average precipitation $\langle P(w/w_c) \rangle$ showing the collapse of the curves for all \hat{T} when column water vapor is rescaled by the critical value w_c for each \hat{T} . Inset: log-log plot of $\langle P \rangle$ versus $(w - w_c)/w_c$ (for $w > w_c$), offset vertically for clarity; straight lines show the fit of (2) for $\beta = 0.23$. b) As in (a) but for the Atlantic.

vertically integrated moisture as outlined in section 6. We use the vertical mass-weighted average (as opposed to integral) in the data analysis to provide more familiar units.

We compute precipitation statistics conditionally averaged on column water vapor w and \hat{T} , for bins of 0.3mm and 1K, respectively, for the tropics from 20N to 20S over the 4.7 year time period. The TMI microwave retrievals at 0.25 degree latitude-longitude resolution are effectively snapshots in time, so the conditionally averaged precipitation rate can be quite high for high w values. We separate out Western Pacific, Eastern Pacific and Atlantic Ocean regions to verify if the aspects we expect to be universal are reproduced in each, and to see the nature of the differences in properties that are expected to change with the large-scale conditions.

a. The pickup in precipitation

The rapid increase in ensemble-average precipitation seen in Fig. 1 as a function of water vapor above the crit-

ical value occurs as in PN, for the revised Hilburn and Wentz (2008) data set used here. In this case, it is seen for each value of \hat{T} and, as hypothesized, the value of the critical water vapor changes as a function of \hat{T} . Curves are shown for values of \hat{T} for which there are sufficient data; parts of the curves with higher scatter are associated with fewer values available for the averages. For instance for $\hat{T} = 274\text{K}$, the upper 10 or so bins have fewer than 10 counts, while bins just below the critical point for the most common temperature, 271K , exceed 10^5 counts. The Eastern Pacific happens to have the widest range of usable temperatures, with the caveat that values associated with the coldest temperature shown, $\hat{T} = 268\text{K}$, tend to be associated with synoptic conditions in which cold temperature mid-latitude systems are intruding into the tropics. A similar pickup is seen in other basins; a Western Pacific case is given in Neelin et al. (2008).

The power law (2) is fit to each curve (linear least squares fit above w_c , iteratively updating w_c). The value of β was set from fits for the most common \hat{T} (270-273K) for the western Pacific and then held constant for all \hat{T} and basins. It is consistent with the value of β determined from radar data in Peters et al. (2008). The double logarithmic inset in Fig. 2a shows that a single value of the exponent β fits well at each temperature. The values of w_c for the eastern Pacific determined from this fit, for $\hat{T}=268\text{K}$ to 274K , are: 56.2, 58.6, 60.9, 63.1, 66.4, 68.2, 70.1 mm, respectively.

Fig. 2a shows the same East Pacific data displayed as a function of the reduced column water vapor w/w_c . The precipitation is also rescaled by the amplitude factor a from (2), but this varies by less than $\pm 5\%$, so the collapse is primarily due to rescaling of w . The $\hat{T}=268\text{K}$ curve deviates slightly from the others below critical, and 268K and 274K have higher scatter due to fewer data counts at high w , but otherwise the curves conform closely to a single dependence in w/w_c . Similar data for the Atlantic (Fig. 2b) illustrates repeatability for other basins. For the Atlantic, there are no occurrences of w high enough to reach the pickup for $\hat{T} = 274$. The quality of the collapse suggests that w_c plays a significant role in the dynamics of the system, and that the reduced variable w/w_c can yield substantial economy in analyzing related statistics. It also indicates that the estimation procedure for w_c works reasonably well for the large data sets here. For smaller data sets, where few counts above criticality prevent fitting the power law, one could still seek such a collapse as a means of obtaining some information regarding w_c .

Comparison with the earlier TMI data set using the Wentz and Spencer (1998) algorithm shows considerable differences in the amplitude a , which also differ in TRMM radar (Peters et al. 2008), but other features including the shape of the pickup and w_c have only modest differences for particular temperatures, suggesting overall robustness of these aspects. The initial part of the pickup has been

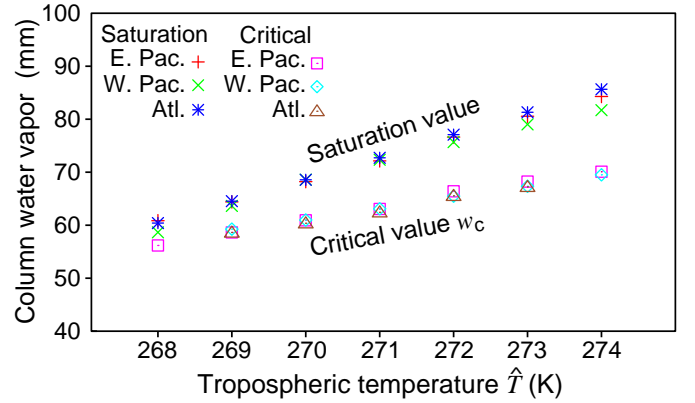


FIG. 3. Critical column water vapor w_c and vertically integrated saturation water vapor $\widehat{q_{\text{sat}}}$ as a function of tropospheric temperature \hat{T} for all basins.

verified with rain gauge and radiosonde data (Holloway and Neelin 2008) but not yet the region far above critical.

b. Critical water vapor as a function of tropospheric temperature

The critical values estimated in Fig. 1 for each basin thus condense crucial information about the onset of strong convection. They are summarized as a function of \hat{T} in Fig. 3. The critical value for the onset of convection increases fairly linearly with \hat{T} , at a rate of about 2.2 mm/K ($\approx 3.6\%$ per K) over the observed range. Values estimated separately for each basin agree well. The TMI algorithm has no information about tropospheric temperature, so the reproducibility among basins increases confidence that the simple temperature dependence is a property of the convective dynamics.

The simplest hypothesis one might consider for the water vapor dependence on temperature is that of saturation. For tropical convection, with deep convective elements separated by descent regions, it has long been known that saturation is not achieved on large scales, but the hope has persisted that there might be some simple relationship to the saturation value. For instance, the Betts-Miller scheme sets w_c to an approximately constant fraction of saturation in (1), and Bretherton et al. (2004) rescale the column water vapor by the column integral of the saturation value. We thus also compute this value, specifically, the vertical integral (200 hPa to the surface pressure) of the saturation specific humidity, $\widehat{q_{\text{sat}}}$, evaluated at each temperature level in the ERA 40 data set and averaged over the same ensemble as was used to determine w_c for each \hat{T} .

When $\widehat{q_{\text{sat}}}$ is displayed as a function of \hat{T} (Fig. 3), the values for different basins agree quite well except for slight variations at the highest temperature values—for which there are fewest counts—which must be the signature of slightly different vertical temperature structures occurring

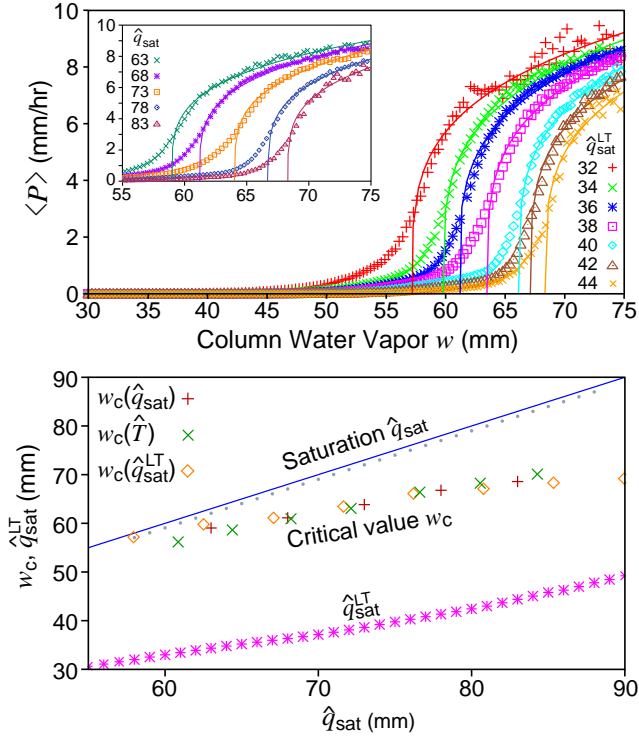


FIG. 4. (a) Pickup of ensemble average precipitation $\langle P \rangle$ as a function of column water vapor w as in Fig. 1 but for 2 mm bins of the lower-troposphere integrated saturation value $\widehat{q_{\text{sat}}}^{LT}$ for the Eastern Pacific; inset same, but for 5mm bins of the vertically integrated saturation value $\widehat{q_{\text{sat}}}$. (b) As in Fig. 3, but for the critical value w_c determined as a function of $\widehat{q_{\text{sat}}}$, $\widehat{q_{\text{sat}}}^{LT}$ and \widehat{T} for the eastern Pacific. Values of $w_c(\widehat{T})$ (repeated from Fig. 3) are plotted at the values of $\widehat{q_{\text{sat}}}$ that correspond to $\widehat{T}=268\text{--}274$ in that figure. Similarly, $w_c(\widehat{q_{\text{sat}}}^{LT})$ is plotted at $\widehat{q_{\text{sat}}}$ values corresponding to $\widehat{q_{\text{sat}}}^{LT}$ binned by $\widehat{q_{\text{sat}}}$ (pink stars). The blue line shows $\widehat{q_{\text{sat}}}$ for reference. Blue dots show $\widehat{q_{\text{sat}}}^{ice}$ (using saturation with respect to ice).

in the ensembles. The column saturation value increases much more rapidly (roughly 6% per K), than the critical value for the convection transition (at 3.6% per K). Column saturation thus clearly does not give a good estimate of the temperature dependence of the onset of strong precipitation (at the scales considered, i.e., larger than individual plumes), and assumptions of a constant fraction of saturation are oversimplified.

c. Comparing measures of tropospheric temperature

In general, we expect that more than one vertical structure of moisture and temperature will affect the transition but we are restricted by the data set to a single vertically integrated measure of moisture. Here, we check for impacts of choosing alternate measures for the leading temperature

effect. Specifically, we examine the same statistics binned by the column integrated saturation value $\widehat{q_{\text{sat}}}$ (200mb to the surface) discussed above, and a lower tropospheric saturation value $\widehat{q_{\text{sat}}}^{LT}$, integrated from 550-875 mb. The latter is associated with a conjecture that entrainment of water vapor in the lower troposphere is a key effect on buoyancy (as discussed in the introduction) and thus that proximity to saturation in this layer is relatively important. While we cannot localize our water vapor data to this layer, we can bin by a temperature measure that reflects conditions in this layer.

As may be seen in Fig. 4, the results parallel those found using \widehat{T} . The pickup in precipitation for both $\widehat{q_{\text{sat}}}^{LT}$ and $\widehat{q_{\text{sat}}}$ (Fig. 4a) is similar to the \widehat{T} binning (Fig. 1), although the exponent fitted here differs slightly (0.26 for all curves). The critical value occurs at a fraction of column saturation that decreases with increasing temperature. To provide a direct comparison of w_c values determined using the different temperature measures, Fig. 4b shows all three on the same plot. This is done by mapping w_c values determined for $\widehat{q_{\text{sat}}}^{LT}$ and \widehat{T} onto $\widehat{q_{\text{sat}}}$ (using the curve of $\widehat{q_{\text{sat}}}^{LT}$ binned by $\widehat{q_{\text{sat}}}$ on Fig. 4b and the $\widehat{q_{\text{sat}}}$ line in Fig. 3). The results for w_c determined using the different measures of temperature are very comparable through the most commonly occurring range.

Also noted in Fig. 4 is a comparison of $\widehat{q_{\text{sat}}}$ for saturation with respect to water (Bolton 1980) to $\widehat{q_{\text{sat}}}^{ice}$ computed using saturation with respect to hexagonal ice below 0C (Murphy and Koop 2005) and averaged on the bins shown. Ice saturation is commonly exceeded in the upper troposphere (Emanuel 1994; Gierens et al. 1999), so $\widehat{q_{\text{sat}}}$ is arguably the more relevant limit, but in any case the difference is small: $\widehat{q_{\text{sat}}}^{ice}/\widehat{q_{\text{sat}}}$ ranges from 98.4% to 98.9% over the range shown for all basins. The behavior of w_c is clearly distinct from both.

In comparing $\widehat{q_{\text{sat}}}$ to w_c , we note the caveat of possible bias from ERA-40 temperatures. While column saturation is a useful foil to show that w_c has more interesting behavior, in practice it is a less good temperature measure for these purposes. Above 272.5, the $\widehat{q_{\text{sat}}}$ - \widehat{T} mapping becomes less trustworthy, with scatter in the relationship. There is a smaller range of $\widehat{q_{\text{sat}}}$ values for which w_c can reasonably be fit, and in general we suspect that $\widehat{q_{\text{sat}}}$ is more dependent on the reanalysis than \widehat{T} due to the larger contribution of the ill-constrained boundary layer temperatures. Using $\widehat{q_{\text{sat}}}^{LT}$ yields a slightly wider range in which good fits are obtained, even compared to \widehat{T} .

The slope of the $\widehat{q_{\text{sat}}}^{LT}$ line in Fig. 4 is roughly parallel to that of w_c . This is potentially consistent with the hypothesis that entrainment in the lower free troposphere tends to prevent deep convection unless the layer is sufficiently close to saturation. This conjecture requires additional assumptions regarding contributions to column water vapor from the boundary layer and the upper tro-

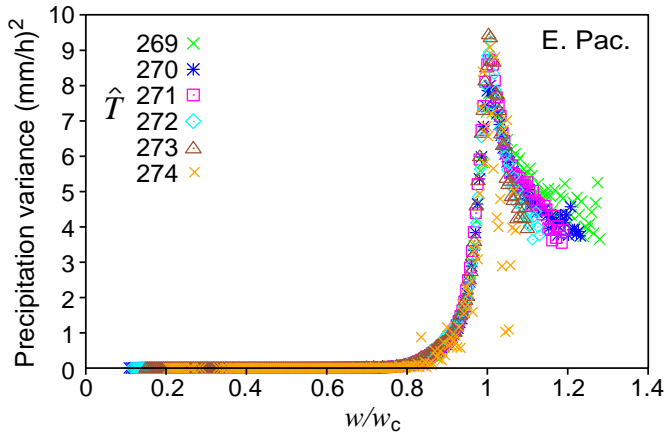


FIG. 5. Variance of precipitation conditioned on w in the Eastern Pacific, showing the collapse of the curves for all \hat{T} when column water vapor is rescaled by the critical value w_c for each \hat{T} .

posphere; for instance, that the former are not closely tied to column temperature, and the latter are sufficiently random that their temperature dependence has less impact than that of the lower free troposphere. We also note the caveat that $\widehat{q_{\text{sat}}}^{LT}$ values are closer to a constant fraction of column saturation (with $\widehat{q_{\text{sat}}}^{LT} \approx 0.44\widehat{q_{\text{sat}}} + 6.6$) than is the w_c dependence. We suggest that $\widehat{q_{\text{sat}}}^{LT}$ holds promise as a useful measure of temperature for future work, as one moves toward situations where temperature is not necessarily coherent through a deep tropospheric layer. For statistics dominated by tropical deep convection zones, \hat{T} and $\widehat{q_{\text{sat}}}^{LT}$ appear approximately equivalent, due to the vertical coherence of temperature (Holloway and Neelin 2007). Most results are thus presented in terms of \hat{T} which allows some simple consequences to be explored in section 6.

d. Precipitation variance collapse

Figure 5 shows the variance of precipitation as a function of column water vapor rescaled by the critical values w_c determined above. PN discusses finite size scaling of the variance. Here we show variance simply as supporting evidence for the critical value determined by fitting the pickup. Although also dependent on the precipitation retrieval, obtaining the peaks in this higher order quantity at very close to the same value helps to boost confidence in the determination of w_c . Furthermore, the sharpness of the peak, with a convex range lying very close on each side, appears inconsistent with having large random errors in the critical value, as will be elaborated in section 4d. The sharpness of the peak is comparable when $\widehat{q_{\text{sat}}}^{LT}$ is used (not shown).

4. Frequency of occurrence and contributions to precipitation

a. Frequency of occurrence

The pickup exhibited in Fig. 1 and Fig. 2 for precipitation, which corresponds to an order parameter, is well known in systems in which the variable corresponding to w , known as the tuning parameter, is externally controlled (Yeomans 1992). In the atmosphere, water vapor is interacting with the precipitation, with a negative feedback of precipitation on water vapor at large scales. There is thus an analogy, as argued in PN, with a class of model systems that exhibit self organized criticality in the following manner. In addition to exhibiting critical phenomena associated with a continuous phase transition, there is a feedback between the order parameter and the tuning parameter that tends to return the system towards the critical region (Tang and Bak 1988; Dickman et al. 1998). The signature of this is seen in the frequency of occurrence of observed water vapor values. For a slowly forced system in which dissipative effects are important only above criticality, the frequency of occurrence tends to peak near the critical point. If strong dissipation occurs above criticality, the system can spend only a small fraction of its time above criticality. For example in the Manna (1991) model, there is an approximately Gaussian distribution peaking just below the critical point (for finite systems).

Figure 6a shows the frequency of occurrence N of each value of w . The crucial characteristic is a sudden drop in the frequency of a occurrence across the critical region. We note that although the critical values were estimated from the pickup in ensemble average precipitation, this sudden drop in N lines up well as a function of the reduced variable w/w_c for each \hat{T} , providing an independent confirmation of the w_c values. The steepest drop begins from just below the critical point, roughly from w/w_c 0.97 to 1.01. Below criticality, the frequency of occurrence is not constrained by loss of water vapor by precipitation processes, and can differ greatly among different \hat{T} , different basins, etc., determined by large-scale dynamics operating on slower time scales (to which we return in section 5).

Above criticality the frequency of occurrence exhibits approximately exponential decay

$$N \propto \exp[-\Lambda(w/w_c)]. \quad (3)$$

There is a substantial literature in tracer transport regarding the circumstances under which distributions are encountered with a Gaussian core and exponential tails (e.g., Pumir et al. 1991; Shraiman and Siggia 1994; Gollub et al. 1991; Pierrehumbert 2000). The sharp drop near criticality in Fig. 6 is potentially consistent with one side of the Gaussian that would be expected from this literature.

The distribution appears even more consistent with this when the frequency of occurrence of precipitating points

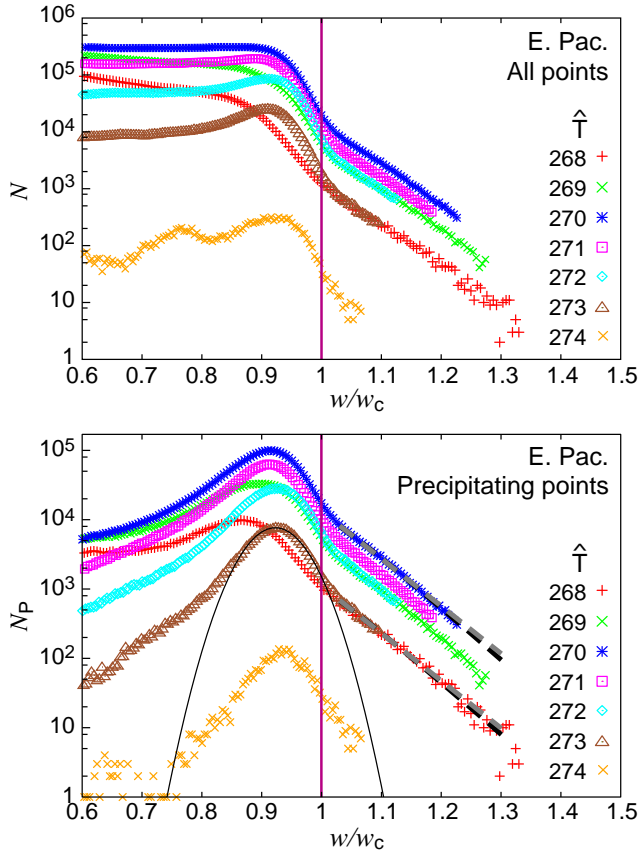


FIG. 6. a) Frequency of occurrence $N(w/w_c)$ as a function of column water vapor rescaled by its critical value w_c for each \hat{T} for the Eastern Pacific (log linear). b) Frequency of occurrence for precipitating points N_P . Curves for a Gaussian core (black curve), and exponential (light dashed lines) and (4) with a next order correction to exponential (dark dashed lines), fitted above $w/w_c=1.03$, are included for reference. Fits of these curves for $\hat{T} = 270$ are repeated with a shift for comparison to $\hat{T} = 268$ and 273 .

[as defined in the Hilburn and Wentz (2008) data set] is examined (Fig. 6b). A leading effect of removing the non-precipitating points is to filter out points in descent regions where the balance is between large-scale descent and evaporation, and where convection has little effect, as further discussed section 5. Above criticality, almost all points are precipitating, so the properties in Fig. 6b are as discussed for Fig. 6a. On the lower side of the critical region, the frequency of occurrence of precipitating points decreases as one moves to lower w . The details of this decrease differ between the lower and higher values of tropospheric temperature as one moves toward low w , and may well depend on the retrieval algorithm or include precipitation not associated with deep convection. The higher \hat{T} curves are roughly consistent with a Gaussian distribution in the critical region, centered at about 0.92, and with a stan-

dard deviation of roughly 0.06. Neither panel of Fig. 6 is normalized because the absolute number of counts at each \hat{T} and w is useful when considering the reliability of other plots. Because the distribution of precipitating points is fairly similar in the central region (with the most counts) normalizing by the number of precipitating points for each \hat{T} tends to collapse the parts of the curves in and above the critical region in Fig. 6b and the above-critical part of Fig. 6a.

While deferring discussion of how to interpret this distribution to section 7, we note here several properties of passive-tracer advection-diffusion models that may be relevant. In analytical/numerical studies Shraiman and Siggia (1994) find such a distribution for departures of tracer concentration from background in a case forced by imposing a large-scale gradient of the tracer, while Pierrehumbert (2000) obtained similar results with a Gaussian stochastic forcing. In addition to a fit to the Gaussian core, we add to Fig. 6b fits for an exponential (3) above 1.03, and also the next order correction to this regime from Shraiman and Siggia (1994):

$$N_P \sim (w^* - w_0^*)^{1/2} \exp[-\Lambda[(w^* - w_0^*)]] \quad (4)$$

where $w^* = w/w_c$, and w_0^* has been matched to the peak of the distribution from the fit of the Gaussian core. A value of $\Lambda \approx 16$ (unitless) characterizes the exponential decay reasonably well for all \hat{T} curves. The fit for $\hat{T} = 270$ is repeated to illustrate the similarity of the slope for other curves. The square-root correction of (4) appears plausible for the slight departure from straight lines although the difference is small over this range [note (4) has been fitted separately, yielding slightly higher $\Lambda \approx 19$]. Other variations of the longtailed behavior, including stretched exponential, have been noted in related systems (e.g. Hu and Pierrehumbert 2001) so (4) should be viewed only as an illustration that modifications to the exponential are no surprise, although here they appear to be small.

In the Shraiman and Siggia (1994) case, the value of Λ is given by the average Lyapunov exponent governing the divergence of trajectories; the width of the Gaussian is inversely related to the log of the Peclet number (VL/κ_0), determined by the diffusivity κ_0 , the velocity scale V and length scale L used to nondimensionalize, the latter being also related to the forced gradient. In Pierrehumbert (2000), the width of the Gaussian region has a dependence on the strength of the forcing. In any case, the forcing (whether by constant gradient, random additions and subtractions, or local resetting to extreme values) is a necessary ingredient for producing long tails. Without forcing, advection-diffusion dynamics eventually leads to Gaussian tracer density distributions (Majda and Kramer 1999).

We note the caveat that passive-tracer advection-diffusion problems are not the only way to produce an exponential distribution. For instance, Gierens et al. (1999) noted

exponential tails in upper tropospheric and lower stratospheric relative humidity and postulated an analogy to results from queuing theory (although we would conjecture forced advection-diffusion as a more likely candidate for that problem as well). An exponential distribution of mass flux has been noted in a cloud resolving model by Cohen and Craig (2006), consistent with theory provided by Craig and Cohen (2006). Furthermore, it is not clear whether horizontal or vertical advection is the more relevant to the distribution seen here. In the vertical, moisture would be subject to a minimum gradient imposed by saturation and the adiabatic decrease in temperature, and one would then expect the distribution to be a property of the convection itself rather than of the large-scale. Clearly, in this case the tracer would not be passive, although the distribution might inherit properties from the simpler problems. Horizontal advection of the water vapor would approximately satisfy conditions of passive-tracer advection and diffusion over long periods of time, with evaporation, large-scale convergence, and punctuation by precipitation events all construed as part of the forcing (as briefly discussed in Neelin et al. 2008). In this case, one might expect the exponential tail to depend on gradients imposed at the large-scale. Another alteration with respect to the simple prototype problems is that the role of diffusivity must be played by transports of water vapor at scales smaller than the 0.25 degree grid on which we observe the water vapor.

Independent of whether forced, diffusive passive-tracer advection provides a good prototype for interpreting the water vapor distribution, we can infer that the long tail above criticality is highly important to the behavior of convection. If the water vapor distribution in Fig. 6 continued to drop as a Gaussian (black curve) above criticality, there would be extremely few occurrences of the high water vapors associated with high precipitation rates. We return to the implications of this in the discussion.

b. Contributions to climatological precipitation

Given the trade-off between the conditionally averaged precipitation increasing rapidly with w above criticality, and the frequency of occurrence dropping off rapidly, it is of interest to quantify where the largest contributions to precipitation lie. Fig. 7 displays the contributions to precipitation computed as follows: the sum over precipitation in each (w, \hat{T}) bin is divided by the count of all points at each \hat{T} ; the result is then normalized by $w_c/(0.3 \text{ mm})$, where 0.3 mm is the bin size, so the area under the curve is proportional to the contribution to precipitation. The value of \hat{T} that has the largest contribution to precipitation depends on the large-scale conditions setting the frequency of occurrence of each temperature and varies from region to region. The key point is that the significant contributions to precipitation are confined to a relatively narrow range just below and above criticality.

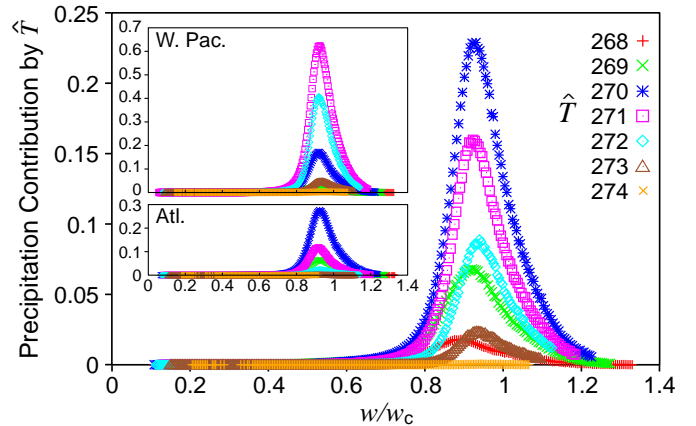


FIG. 7. Contributions to ensemble-average precipitation as function of w/w_c for each \hat{T} . The amplitudes are scaled such that the area under the curve is proportional to the contribution of that \hat{T} to climatological precipitation averaged over the region. Main panel: Eastern Pacific; Insets: Western Pacific and Atlantic.

For example, for the eastern Pacific: for the most common temperature, $\hat{T} = 270$, about 25% of the rainfall occurs above the critical point, with 95% occurring above $0.8w_c$. The same applies for the average over the whole $\hat{T} = 268\text{--}274$ range. For warmer values, $\hat{T} = 272\text{--}274$, the fraction of rain occurring above criticality increases slightly (27–28%), with 98–99% of rainfall occurring above $0.8w_c$. The value $0.8w_c$ is used for reference because it is approximately 2 standard deviations (of the fit to the Gaussian core of N_P in section 4a) below the center of the Gaussian core, and roughly corresponds to the switch to the long tail of precipitating points on the low w side.

One implication is that the part of $\langle P(w/w_c) \rangle$ curve below criticality is an important contribution in computing the climatological precipitation. The behavior of this part of the pickup is non-universal and so harder to characterize based on statistical mechanics prototypes. Section 4d discusses some possibilities, including the question of whether the width of this region is a fundamental characteristic of moist convection, or results from imperfect characterization of the critical value.

c. Fraction of precipitating points

The ensemble average precipitation as a function of w (Fig. 1) can be written in terms of the fraction of precipitating points times the average precipitation for points that are precipitating, so we have examined these two quantities separately (not shown). For stochastic convection representations, one might have hoped that the transition would occur primarily in the probability of precipitation. This would potentially allow strong convection to be approximated as a sum of many small “convection units”. At

the scale of the data used here, $(25 \text{ km})^2$, this does not hold: the power law pickup is primarily in the average over precipitating points, while the probability of precipitation approaches one near w_c . However, this statistic will depend strongly on the horizontal averaging, so it remains possible that this could change at the scale of the individual updraft.

d. The region below the critical point

Several effects may contribute to the behavior of the pickup in the critical region just below w_c . We use item (iii) of the following, listing the others for completeness. In each case, we consider effects that can potentially contribute to the departure from the thermodynamic limit of infinite system size for a continuous phase transition, where the order parameter (here precipitation) is zero below the critical value, and governed by (2) above.

- (i) For systems of finite-size, the smooth pickup below the critical point qualitatively resembles that seen in Fig. 1. Thus, a leading possible contributor to the smooth pickup behavior is the analogue of finite-size effects. For instance, if the relevant units of the convection process are convective plumes, a pixel of (25 km^2) does not contain many of them, so this behavior would be expected.
- (ii) A smooth pickup just below the critical value also occurs in the near neighborhood of a critical point in models where there is a conjugate field, such as an external magnetic field in an Ising model (Yeomans 1992). When this field is sufficiently weak, the critical properties of the phase transition can be observed. Many factors affect deep convective plumes, and we only control for \hat{T} or w from states that the observed system visits, so it is very possible that we are observing the near neighborhood rather than the precise critical point. If so, one could postulate finding a closer approximation to critical behavior in a convection resolving model, by altering parameters, e.g., affecting microphysics or radiative descent between clouds.
- (iii) Even in the absence of a conjugate field, the position of the critical point may be affected by further variables that are currently not accounted for. Non-observed variables may act as a random contribution to w_c , as elaborated below.
- (iv) Precipitation may have more complicated dependences than the ideal order parameter. The convection transition is hypothesized to be associated with updraft kinetic energy generated from buoyancy; the step to precipitation requires aggregation of hydrometeors, and the rainfall may not all occur locally. If so, then

using a measure of convective rainfall, excluding rain associated with anvils, might yield an even sharper pickup.

Regarding item (iii), It is reasonable to hypothesize that w_c should depend not only on \hat{T} but on other vertical degrees of freedom, such as variations in boundary layer moisture and temperature. Noting that our transformation to a reduced water vapor w/w_c can be viewed as a nonlinear version of a local rotation in the w - \hat{T} plane, a similar procedure could be applied using other vertical degrees of freedom in water vapor and temperature to more accurately define w_c if we had observations of these quantities.

In the absence of these observations, we can consider their impact by writing $w_c^{\text{true}} = (w_c - \xi)$, where ξ represents the variation in the true critical value w_c^{true} about our estimate $w_c(\hat{T})$ due to these non-observed variables. For small variations near w_c^{true} , the reduced variable scaled by w_c^{true} becomes approximately $w^* + \xi^*$, where each is scaled by w_c . Letting \bar{P} and σ_P^2 denote the mean and variance of precipitation conditioned on reduced water vapor (with the true w_c), and taking the expectation over ξ , the quantities we have been displaying can be regarded as:

$$\int \bar{P}(w^* + \xi^*)p(\xi^*)d\xi^*, \quad \text{and} \quad \int \sigma_P^2(w^* + \xi^*)p(\xi^*)d\xi^*, \quad (5)$$

where $p(\xi^*)$ is the probability density function for ξ^* . Sufficiently above criticality, if the distribution is approximately symmetric and narrow enough that the curvature of \bar{P} is negligible over the range of high probability, then impact of random zero-mean error on the average precipitation will be small. Below criticality, excursions of ξ^* will tend to increase the estimated $\langle P \rangle$, especially approaching w_c . The impact on σ_P^2 of any ξ^* distribution that tends to be broad near its mean will be to broaden the sharp peak. Indeed, comparing to the results from PN, this is exactly what occurred when we did not control for \hat{T} . The standard deviation of \hat{T} over the eastern Pacific is about 1K, translating to a roughly 4% random error in w_c . The broadening of the precipitation variance peak in PN relative to current appears commensurate with this.

Examining the variance in Fig. 5 in this light, it is remarkable how sharp the peak is (especially given that effects (i) and (ii) contribute some width at a fundamental level). It would appear implausible that the random errors to w_c could have a standard deviation of much more than 1-2 percent. Thus, at least for deep convective regions that dominate the statistics here, we can infer that column integrated water vapor and temperature are—fortunately—very reasonable leading variables for identifying the transition.

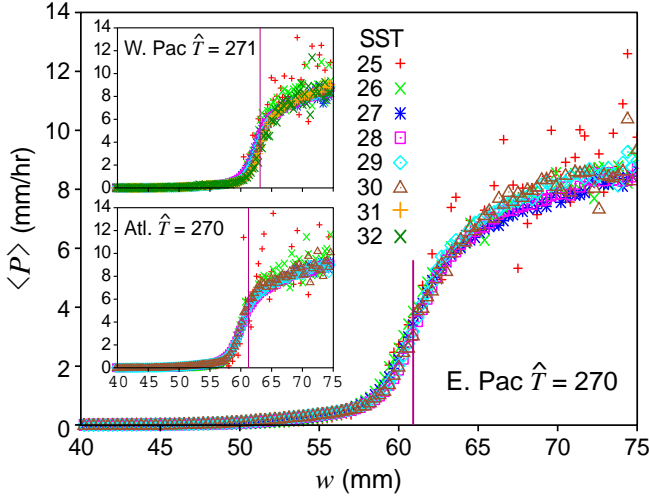


FIG. 8. Ensemble average precipitation $\langle P(w, \hat{T}, SST) \rangle$ for a given \hat{T} and various SST (Note w is shown from 40mm up and is not rescaled.) For each basin, the value of \hat{T} with the largest contribution to total precipitation is shown. Main panel: Eastern Pacific for $\hat{T} = 270$; (SST 25C-30C); Insets show the Western Pacific for $\hat{T} = 271$ K (SST 25C-32C) and the Atlantic for $\hat{T} = 270$ K (SST 25C-30C). Vertical lines indicate the critical values w_c .

5. The role of SST

From the point of view of examining the robustness of statistics such as the column water vapor probability density function, SST provides a proxy for changing large-scale conditions. We also wish to determine the extent to which the present analysis can separate the role of large-scale effects from aspects such as the critical value which we would like to attribute to the properties of convection itself.

There is a long history of empirically linking precipitation on monthly and longer time scales to SST (Bjerknes 1966; Ramage 1977; Webster 1981; Gill and Rasmusson 1983; Graham and Barnett 1987; Neelin and Held 1987). This relationship is sometimes phrased in terms of a threshold SST value for convection (Graham and Barnett 1987; Folkins and Braun 2003). From first principles, the onset of convection depends on atmospheric temperature and moisture through column conditional stability. SST affects these via surface heat and radiative fluxes, which form part of the slow driving for the circulation. While SST is fundamentally a large-scale forcing, it is not clear in advance how to expect the role of SST to appear in these diagnostics. The SST potentially could be a proxy for boundary layer moist static energy (Brown and Bretherton 1997; Raymond 2000), which we do not observe directly here (using w and vertically integrated temperature measures) but which might well affect the critical value for the onset of

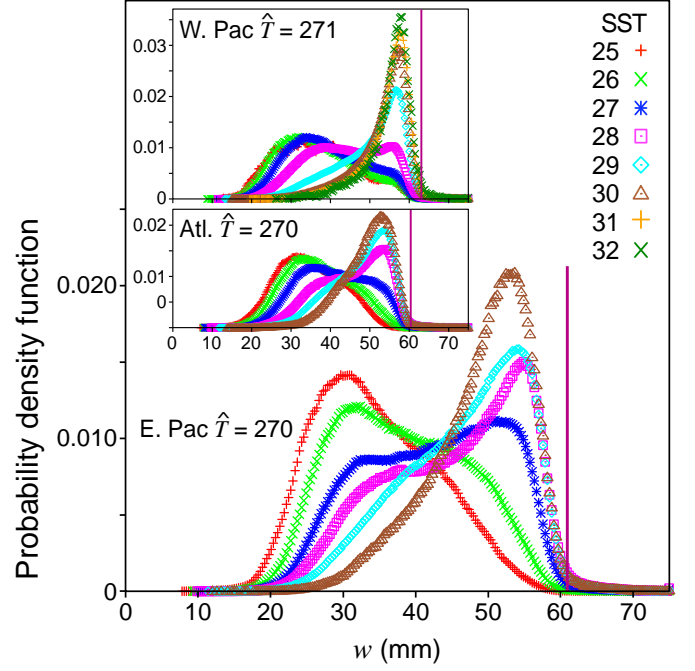


FIG. 9. Probability density function of w (frequency of occurrence normalized by total number, i.e. the sum over w bins=1, at each \hat{T} , SST) corresponding to the curves in Fig. 8, for the Eastern Pacific (main figure), with insets showing similar behavior for Western Pacific and Atlantic. Vertical lines indicate the critical values w_c .

convection.

To examine the dependence on SST we calculated conditional averages for bins of all three variables: w , \hat{T} , and SST by bins of 1C. Choosing the values of \hat{T} for which the largest contributions to precipitation occur, Fig. 8 displays the ensemble average precipitation as a function of w and SST. The pickup of precipitation in Fig. 8 is unequivocal: it depends very little on SST. In the western Pacific, a very slight change in the pickup can barely be seen between the curves, but it is less than 1mm from SST=27C to SST = 32C. The higher scatter for the highest and lowest values of SST is because there are very few occurrences from which to compile the averages. The available sample for each SST value varies from basin to basin; for the warm western Pacific curves for 31-32C are included. The lack of dependence of w_c on SST is reproduced for neighboring values of \hat{T} . This appears to hold generally, with the caveat that a few cases of small sample size may be found that deviate slightly under unusual combinations of cold SST and warm \hat{T} (presumably corresponding to unusual large-scale conditions).

How then does the SST exert its effect on climatological precipitation? The answer may be seen in the frequency of occurrence displayed in Fig. 9. As SST increases, the system spends more and more of its time at the higher

values of column water vapor. This larger forcing would in part be due to higher evaporation, but also due to the effects of increased surface energy flux over warmer SST, tending to favor atmospheric convergence. For the higher values of SST, the sharp drop in residence time near the critical value of water vapor, associated with the onset of strong convection, is particularly clear.

At lower SST, the curves maximize at much lower values of column water vapor. The w value at which this occurs would be set by the balance of the moisture divergence versus evaporation characterizing descent regions. Some intermediate values of SST exhibit double maxima, corresponding to some fraction of the occurrences being in the descent regime and some in the ascent regime, where moisture convergence causes water vapor to increase until the onset of sufficiently strong precipitation.

Fig. 10 shows the frequency of occurrence distribution for water vapor for precipitating points at different values of SST (those with sufficient counts above criticality). The Gaussian core near the critical region and exponential tail above criticality noted in Fig. 6 are very reproducible. The distribution at low w varies greatly, especially at low SST (where any rain is unlikely to be deep convective), consistent with the expectation that other behavior governs regions far from criticality. The exponential decay slope Λ is typically close to the reference value from Fig. 6b for $\hat{T}=270$ K in the eastern Pacific, averaged over all SST. The slope exhibits slight differences between the lowest and highest SST values. The range is typified by the fits for SST= 27C and 31C in Fig. 10b; these differ by only $\pm 9\%$ from the reference value. In the Shraiman and Siggia (1994) example, such differences could be produced by changes in the mean Lyapunov exponent, or the velocity scale or length scale used to non-dimensionalize it, so some variation from region to region might be expected. The slightly steeper slope at high SST may be consistent with smaller SST gradients that typify these regions—horizontal advection is less likely to bring in high water vapor values. However, given the large range of large-scale climatological conditions spanned by these SST values in Eastern and Western Pacific, the small range of variation in the slope of the exponential tail is remarkable. Furthermore, the steep drop of the Gaussian core lines up with the critical value in all cases. Thus while below criticality the system can produce a range of behavior—notably spending a larger fraction of the time nonprecipitating for lower SST (Fig. 9)—near and above criticality the behavior is highly constrained by the interaction with convection.

Overall, these results produce a surprisingly clear partition between the role of tropospheric temperature and column water vapor and the role of SST. While the critical value depends on both w and \hat{T} , the role of the SST is almost entirely in the forcing of the system, affecting the frequency of occurrence of sufficiently high water vapor to

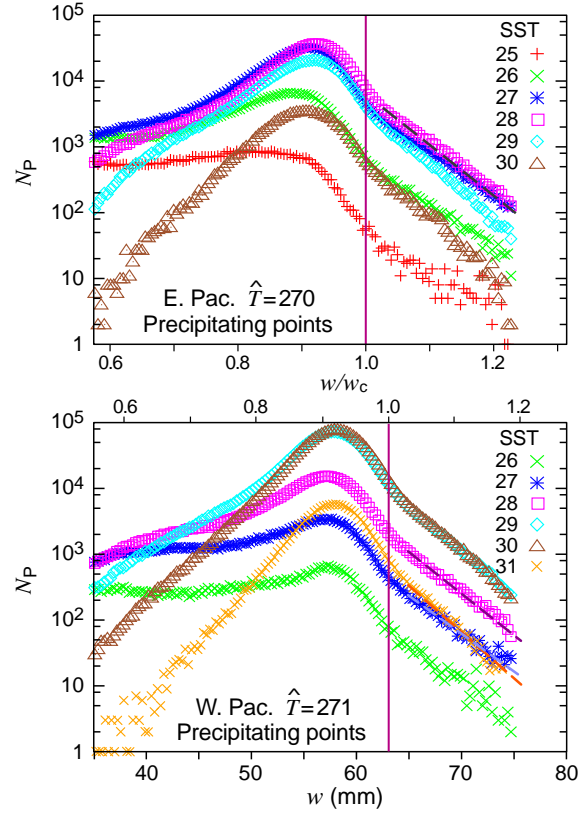


FIG. 10. Frequency of occurrence of w for precipitating points N_P with log-linear scale as in Fig. 6b but for a given \hat{T} bin and several SST bins (SST=25–30C) for (a) Eastern and (b) Western Pacific. The w axis is the same for both Eastern and Western Pacific, with a scale for w/w_c provided for each that depends on the $w_c(\hat{T})$ for the respective \hat{T} . Vertical lines indicate the critical values w_c . Black dashed lines in the exponential range at SST=28C in both panels provide the slope from Fig. 6b (eastern Pacific, $\hat{T}=270$ K, all SSTs). Gray and orange dashed lines show fits to SST = 27C and 31C in (b).

precipitate.

6. Simple considerations for parameterization

Consider the vertically integrated equations for temperature T and specific humidity q

$$\partial_t \hat{T} + \text{LS}_T = \widehat{Q}_c \quad (6)$$

$$\partial_t \hat{q} + \text{LS}_q = -\widehat{Q}_q \quad (7)$$

where LS_T and LS_q denote the large-scale forcing, including both dynamical and radiative effects, and \widehat{Q}_c and \widehat{Q}_q denote the convective heating and moisture sink due to sub-grid scales, respectively. For compactness of notation, we absorb the heat capacity and the latent heat of condensation into T and q , respectively, and let $\hat{\cdot}$ denote a vertical

integral instead of vertical average, so that $w = \hat{q}$. If horizontal transport of water substance by the small scales is negligible

$$\widehat{Q}_c = \widehat{Q}_q \approx P \quad (8)$$

where P is precipitation. In a traditional convective parameterization, the convective heating is considered to be an ensemble average over many convective elements, represented as a function of large-scale temperature and moisture. For the vertical mean, we now have such a function, estimated empirically. Define this function $\mathcal{P}(w, \hat{T})$ as the average of the collapsed curves in Fig. 2, redimensionalized by $a(\hat{T})$. For values more than about 0.3 mm above the critical point, we can approximate this by (2). Noting that $aw_c^{-\beta}$ does not have a strong dependence on \hat{T} , we can approximately write this function as $\mathcal{P}(w - w_c(T))$. This will be useful below and makes clear the qualitative resemblance to the Betts-Miller parameterization (1).

For the range of \hat{T} examined here, we can approximate the w_c dependence seen in Fig. 3 as

$$w_c \approx w_c^r + \gamma_c(\hat{T} - T^r) \quad (9)$$

where w_c^r and T^r are constant reference values, and $\gamma_c \approx 0.70$ (non-dimensional since w and \hat{T} here have the same units; calculated as $L(c_p \times 8.15 \text{e3 kg/m}^2)^{-1} \times 2.3 \text{ mm/K}$ from Fig. 3). We then can then combine (7)– $\gamma_c \times$ (6) to form an equation for the time evolution of $w - w_c(\hat{T})$:

$$\partial_t(w - w_c) + \text{LS} = -(1 + \gamma_c)\mathcal{P}(w - w_c) \quad (10)$$

This is the equivalent of the convective available potential energy (CAPE) decay equation occurring in the Zhang and McFarlane (1995) parameterization, and has an explicit counterpart in the Betts-Miller parameterization (Neelin and Zeng 2000). We can thus examine the time decay characteristics for a case where the system has been perturbed to high w , such that the precipitation term is much larger than the LS term. For the Betts-Miller case, with $\mathcal{P}(w - w_c(\hat{T}))$ given by (1), exponential decay occurs with timescale $\tau_c/(1 + \gamma_c)$.

If \mathcal{P} is given by (2), then while LS is negligible

$$\partial_t w_* = -a_* w_*^\beta \mathcal{H}(w_*), \quad (11)$$

with $w_* = (w - w_c)/w_c$, $a_* = a(1 + \gamma_c)/w_c$ and \mathcal{H} the Heaviside step-function. Above w_c there exists a power-law solution

$$w_*(t) = [(1 - \beta)a_*(t_c - t)]^{\frac{1}{1-\beta}}, \quad (12)$$

$$t_c = w_*(0)^{\beta-1} [a_*(1 - \beta)]^{-1}$$

where t_c is the time it takes to decay to a value of w arbitrarily close to w_c . Power law decay has been previously examined in the context of approaches to convective QE (Yano et al. 2000, 2001), but in the case of negative exponent, i.e., slow approach to equilibrium.

Here, the decay to w_c occurs in finite time. For instance, for initial $w_*(0) = 0.2$ (20% above criticality), $t_c \approx 1$ hr. The part of the ensemble mean curve below criticality would imply that the decay then continues toward lower w , but at a decreasing rate, until the precipitation can be balanced by the large-scale forcing.

For purposes of constraining or improving convective parameterizations in general circulation models, we do not suggest direct use of the closure above. Rather, this ensemble mean parameterization based on the empirical curve makes more precise the relationship to traditional QE schemes. It exhibits the tendency to return the system to below the critical point, but with no single decay time and in finite time. Obtaining high variance near the critical point and a slowly decaying distribution above criticality requires departures from the ensemble mean assumptions (for instance, the large-scale forcing may not always be small, or the finite-time convective process may overshoot to below criticality). It may be possible to devise a stochastic scheme, motivated by simple systems that exhibit these properties (e.g., reviewed in Neelin et al. 2008) to reproduce the observed properties. The closed system illustrated here for vertical average properties can provide guidance in designing processes for intermediate complexity models. The return to criticality in finite time appears consistent with episodic behavior, with finite convective events rather than smooth exponential decay toward equilibrium, even if the large-scale changes slowly.

7. Discussion

a. Tropospheric temperature dependence

Here some of the statistics of tropical precipitation shown in PN to match universal properties associated with critical phenomena are used to probe the physics of tropical convection empirically. Satellite microwave retrievals for column water vapor w and precipitation are used with ERA40 reanalysis temperatures—caveats and concurrent studies with other data sets are noted in the text. The pickup of the ensemble average precipitation $\langle P \rangle$ as a function of column water vapor is shown to depend on tropospheric temperature, as expected from convective parameterizations. Fitting the power law dependence of $\langle P \rangle$ above the critical water vapor w_c , permits an empirical determination of this critical value as a function of column tropospheric temperature. The results are highly reproducible for different measures of tropospheric temperature: vertically integrated saturation value, vertically averaged tropospheric temperature, and lower free-tropospheric saturation value (with the latter two yielding slightly cleaner results). Rescaling w by w_c collapses the precipitation pickup curve $\langle P \rangle(w/w_c)$ for the various tropospheric temperatures. A similar collapse occurs to a good approximation for the sharp peak that occurs in the precipitation variance as a function of w/w_c ,

and for the drop in frequency of occurrence of column water vapor discussed below.

The collapse of precipitation statistics implies that the empirically determined critical value as a function of temperature is an important quantity for analysis of precipitation statistics, and potentially useful in validation of convection schemes. This temperature dependence is found to be substantially different from that of column saturation—the onset of strong convection occurs at a fraction of column saturation that decreases with temperature. This implies that using column saturation to scale w would not provide a good collapse of precipitation statistics at these space and time scales, although this had previously seemed a plausible guess (e.g., Bretherton et al. 2004).

Although we do not have a full explanation for the temperature dependence, a leading conjecture is that it may be controlled by near-saturation in the lower free troposphere. The effect of lower free tropospheric water vapor on deep convection (Sherwood 1999; Parsons et al. 2000; Tompkins 2001; Derbyshire et al. 2004) has been quantified in terms of the entrainment through the lower troposphere required to match onset of convective instability to the precipitation pickup with w (Holloway and Neelin 2008). The relationship of w_c to vertically integrated saturation through the lower troposphere appears consistent with this. If so, it may be possible to match the empirically determined temperature dependence of the critical point with suitably chosen entrainment processes in parameterized convective plumes.

The critical surface as a function of water vapor and temperature is here examined in terms of column integrated water vapor and temperature quantities. A priori, one anticipates that other thermodynamic variables, i.e., other vertical degrees of freedom in moisture and temperature, can affect the critical value. The rescaling by $w_c(\hat{T})$ is locally similar to a rotation of the critical surface to produce a single variable orthogonal to it in the w - \hat{T} plane. We can foresee using similar techniques with other data sets to explore other vertical degrees of freedom that might affect the transition, such as the boundary layer versus lower tropospheric water vapor—with the caveat that large amounts of data for precipitating conditions are required due to slow convergence of statistics above criticality where frequency of occurrence is low.

The cleanness of the results obtained here with just vertically integrated values suggests that relatively few vertical degrees of freedom can yield a good approximation in characterizing the onset of convection. In particular, the sharpness of the variance peak suggests that other vertical structures must not typically be yielding critical point variations by much more than the order of a percent. Physically, this appears consistent with the argument that high water vapor is required in the lower free troposphere as well as the boundary layer for entraining plumes to remain

sufficiently buoyant for the onset of deep convection to occur. If the transition occurs only when there is a moist layer through the lower troposphere, it would explain why column water vapor can determine the transition at this precision.

b. The water vapor distribution near criticality and hypothesized interpretation

The frequency of occurrence (or, when normalized, the probability density function) of a given column water vapor value has a characteristic rapid decrease as the system approaches the critical point. Slightly above criticality, the distribution of column water vapor values becomes exponential, so that the decay above criticality is less rapid than just near criticality. When the column water vapor distribution is displayed for precipitating points, the behavior appears to be consistent with a Gaussian core with exponential tails noted in tracer transport problems, as discussed in section 4a. Here, the distribution is not symmetric on the low water vapor side (especially for lower tropospheric temperature values). The key aspect is the behavior on the high water vapor side, which is very reproducible for various tropospheric temperature values. The steep drop in probability of occurrence on the upper side of the Gaussian core lines up neatly with the critical value, with the exponential tail above criticality.

An interpretation of the observed distribution near and above the critical point may be hypothesized in two parts: one regarding the shape, and one regarding the relation to criticality. Similar distributions are produced in forced passive-tracer advection-diffusion problems (Gollub et al. 1991; Shraiman and Siggia 1994; Pierrehumbert 2000). Forcing in the observed case occurs in several forms: a large-scale input by evaporation and eventual loss at convective scales by precipitation; in between there is a three-dimensional transport problem. While several parts of the problem are more complex than the forced convection-diffusion prototypes, the essential conditions are sufficiently similar that this appears a plausible explanation for the observed transition from Gaussian core to exponential tail. One then needs to explain the relationship of this distribution to the critical value for the onset of strong precipitation.

The observed alignment of the steep drop associated with the upper side of the Gaussian with the critical point can then be explained as follows. This is a variant of the arguments applied to self organized criticality (Dickman et al. 1998) for non-equilibrium systems with a feedback that moves them back toward a critical point (specifically, an absorbing state of a related system) when an external forcing acts to move them above it. For large-scale forcing that tends to increase column water vapor, sufficient occurrences in the critical region and above are required to provide the balancing precipitation. Consider shifting

the distribution toward higher water vapor until there is sufficient sink; if the strong but relatively rare precipitation events in the long tail above criticality cannot provide enough moisture sink, then the balance will very likely occur when the rapid increase associated with the upper edge of the Gaussian core approaches the critical point. The rapid change in frequency of occurrence along this side of the Gaussian core implies that this part of the distribution cannot be pushed very far into the critical region without strong moisture input to the system. Furthermore, the crossover from the Gaussian core to the exponential tail may depend on the forcing (with a relatively larger core for weak forcing), and this may be hypothesized to further constrain the crossover from Gaussian to exponential to occur near the critical point.

A significant feature that distinguishes this from some model systems exhibiting self organized criticality is the exponential tail. This yields much more frequent occurrences of high precipitation rate than if the distribution continued to drop as a Gaussian above criticality. This property is also what permits us to observe the region above criticality in the available data.

A large fraction of the precipitation occurs near and above the critical point. About 25% occurs above the critical point. If one uses two standard deviations below the peak of the Gaussian core as an indicator of the lower bound of the critical region, about 95% of the precipitation occurs above this.

Pragmatically, the distribution above criticality provides a means of quantifying excursions into the strongly convective regime that can be useful in testing models, many of which have insufficient occurrence of strong precipitation (Trenberth et al. 2003; Dai 2006; Wilcox and Donner 2007), or in constructing stochastic convective schemes. The sharp drop at criticality provides an additional criterion in empirically mapping the convection transition in the water vapor-temperature plane.

c. Role of SST

These characteristics of the column water vapor distribution can further be used, at least in some cases, to distinguish between properties of the convection itself and properties of the large-scale forcing. The effects of SST provide an example of the latter. SST is found not to have a strong effect on the critical pickup of precipitation. This can appear at first counterintuitive because the well-known tendency of climatological tropical precipitation to increase over regions of warm SST has sometimes been phrased as if there were some threshold value of SST at which the onset of convection occurs (Graham and Barnett 1987).

Here, we find that the effect of SST on the climatological precipitation occurs via the frequency of occurrence. Over regions of warm SST, the system spends a larger fraction of its time near criticality. This is consistent with

large-scale forcing typically being larger over warmer SST, while the critical value and associated precipitation pickup is a property of the convection itself, and depends only on the tropospheric water vapor and temperature. This partition is surprisingly clear in the empirical results. Furthermore, the exponential tail of the column water vapor distribution above criticality varies little over SST values spanning a large range of large-scale conditions.

d. Practical applications

Finally, we summarize briefly some potential near-term practical applications. For empirical studies, the clean separation between the role of tropospheric temperature and column water vapor versus the role of SST might be adapted to examine other large-scale effects. For instance, inflow of air from a dry region should affect the frequency of occurrence, not the critical value.

For model evaluation, we argue that several of the diagnostics here can be used or adapted (discussion with several modeling groups is underway). In particular, the empirical temperature dependence of the critical point, and the behavior of the precipitation pickup and frequency of occurrence of reduced water vapor near and above criticality are of interest. Such comparison appears particularly relevant given the role that the threshold for convection and the change of water vapor and precipitation characteristics with temperature plays in questions of precipitation change under global warming and interannual teleconnections (e.g., Chiang and Sobel 2002; Allen and Ingram 2002; Neelin et al. 2003; Trenberth et al. 2003; Held and Soden 2006).

High-resolution models may be analyzed for direct comparison to the statistics presented here. Requirements include (i) sufficiently long time series to acquire stable statistics in the high w tail (short time series tend to yield only the beginnings of the precipitation pickup before the standard error becomes large as frequency of occurrence drops); and (ii) snapshot output of precipitation and related quantities that best compares to the extremely short time of the satellite instrument scan (many models standardly output accumulations over several hours, which tends to average over the phenomenon of interest here).

Although low-resolution models may not reproduce the high rainfall rate part of the curve in Fig. 1, there are several things that can be compared. Because the transition as a function of water vapor and temperature is built into convective parameterizations, some version of the pickup will occur in the models. Even without being able to fit the power law, one can potentially perform a collapse similar to that seen in Fig. 2 (i.e., finding the rescaling required to minimize tropospheric temperature dependence) as a means of obtaining information regarding w_c for models. The water vapor distribution, in particular the decrease in

frequency of occurrence in the range of water vapor where precipitation increases, and whether the models produce the observed exponential tail, is equally of interest. Besides yielding information about model performance, such comparison can potentially answer questions regarding how the interaction of large scales with convection produces some of the features noted empirically here.

Acknowledgments.

This work was supported under National Science Foundation ATM-0082529 and National Oceanic and Atmospheric Administration NA05-OAR4310007 and NA08OAR4310882. JDN acknowledges sabbatical support from the J. S. Guggenheim Foundation. TMI data are produced by Remote Sensing Systems and sponsored by the NASA Earth Science Reason Discover Project. We thank C. Bretherton, C. Holloway, B. Legras for discussions and J. Meyerson for graphical support.

REFERENCES

- Allen, M. R. and W. J. Ingram, 2002: Constraints on future changes in climate and the hydrologic cycle. *Nature*, **419**, 224–232.
- Arakawa, A., 2004: The cumulus parameterization problem: Past present and future. *J. Climate*, **17**, 2,493–2,525.
- Arakawa, A. and W. H. Schubert, 1974: Interaction of a cumulus cloud ensemble with the large-scale environment Part I. *J. Atmos. Sci.*, **31**, 674–701.
- Austin, J. M., 1948: A note on cumulus growth in a non-saturated environment. *J. Meteor.*, **5**, 103–107, doi:10.1175/1520-0469(1948)005<0103:ANOCGI>2.0.CO;2.
- Bechtold, P., M. Köhler, T. Jung, F. Doblas-Reyes, M. Leutbecher, M. J. Rodwell, F. Vitart, and G. Balsamo, 2008: Advances in simulating atmospheric variability with the ECMWF model: From synoptic to decadal time-scales. *Quart. J. Roy. Meteor. Soc.*, **134**, 1337–1351, doi:10.1002/qj.289.
- Betts, A. K. and M. J. Miller, 1986: A new convective adjustment scheme. Part II: Single column tests using GATE wave, BOMEX, ATEX and arctic air-mass data sets. *Quart. J. Roy. Meteor. Soc.*, **112**, 693–709.
- Biasutti, M., A. H. Sobel, and Y. Kushnir, 2006: AGCM precipitation biases in the tropical Atlantic. *J. Climate*, **19**, 935–958.
- Bjerknes, J., 1966: A possible response of the atmospheric Hadley circulation to equatorial anomalies of ocean temperature. *Tellus*, **18**, 820–829.
- Bolton, D., 1980: The computation of equivalent potential temperature. *Mon. Wea. Rev.*, **108**, 10461053.
- Bretherton, C. S., 2007: Challenges in numerical modeling of tropical circulations. *The Global Circulation of the Atmosphere*, T. Schneider and A. H. Sobel, Eds., Princeton University Press, Princeton, 302–330.
- Bretherton, C. S., M. E. Peters, and L. Back, 2004: Relationships between water vapor path and precipitation over the tropical oceans. *J. Climate*, **17**, 1517–1528.
- Bretherton, C. S. and A. H. Sobel, 2002: A simple model of a convectively-coupled walker circulation using the weak temperature gradient approximation. *J. Climate*, **15**, 2907–2920.
- Brown, R. G. and C. S. Bretherton, 1997: A test of the strict quasi-equilibrium theory on long space and time scales. *J. Atmos. Sci.*, **5**, 624–638.
- Buizza, R., M. Miller, and T. N. Palmer, 1999: Stochastic representation of model uncertainties in the ECMWF ensemble prediction system. *Quart. J. Roy. Meteor. Soc.*, **125**, 2887–2908.
- Chiang, J. C. H. and A. H. Sobel, 2002: Tropical tropospheric temperature variations caused by ENSO and their influence on the remote tropical climate. *J. Climate*, **15**, 2616–2631.
- Christy, J. R., R. W. Spencer, and W. D. Braswell, 2000: MSU tropospheric temperatures: Dataset construction and radiosonde comparisons. *J. Atmos. Oceanic Technol.*, **17**, 1153–1170.
- Cohen, B. G. and G. C. Craig, 2006: Fluctuations in an equilibrium convective ensemble. Part II: Numerical experiments. *J. Atmos. Sci.*, **63**, 2005–2015, doi:10.1175/JAS3710.1.
- Craig, G. C. and B. G. Cohen, 2006: Fluctuations in an equilibrium convective ensemble. Part I: Theoretical formulation. *J. Atmos. Sci.*, **63**, 1996–2004, doi:10.1175/JAS3709.1.
- Dai, A., 2006: Precipitation characteristics in eighteen coupled climate models. *J. Climate*, **19**, 4605–4630.
- Derbyshire, S. H., I. Beau, P. Bechtold, J.-Y. Grandpeix, J.-M. Piriou, J.-L. Redelsperger, and P. M. M. Soares, 2004: Sensitivity of moist convection to environmental humidity. *Quart. J. Roy. Meteor. Soc.*, **130**, 3055–3079.
- Dickman, R., A. Vespignani, and S. Zapperi, 1998: Self-organized criticality as an absorbing-state phase transition. *Phys. Rev. E*, **57**, 5095–5105.
- Emanuel, K. A., 1991: A scheme for representing cumulus convection in large-scale models. *J. Atmos. Sci.*, **48**, 2313–2335.
- Emanuel, K. A., 1993: The effect of convective response time on WISHE modes. *J. Atmos. Sci.*, **50**, 1763–1775.
- Emanuel, K. A., 1994: *Atmospheric Convection*. Oxford University Press, New York, 580 pp.
- Emanuel, K. A., J. D. Neelin, and C. S. Bretherton, 1994: On large-scale circulations in convecting atmospheres. *Quart. J. Roy. Meteor. Soc.*, **120**, 1111–1143.
- Folkens, I. and C. Braun, 2003: Tropical rainfall and boundary layer moist entropy. *J. Climate*, **16**, 1807–1820.
- Gierens, K., U. Schumann, M. Helten, H. Smit, and A. Marenco, 1999: A distribution law for relative humidity in the upper

- troposphere and lower stratosphere derived from three years of MOZAIC measurements. *Ann. Geophysicae*, **17**, 1218–1226.
- Gill, A. E. and E. M. Rasmusson, 1983: The 1982–1983 climate anomaly in the equatorial Pacific. *Nature*, **306**, 229–234.
- Gollub, J. P., J. Clarke, M. Gharib, B. Lane, and O. N. Mesquita, 1991: Fluctuations and transport in a stirred fluid with a mean gradient. *Phys. Rev. Lett.*, **67** (25), 3507–3510, doi:10.1103/PhysRevLett.67.3507.
- Graham, N. E. and T. P. Barnett, 1987: Sea surface temperature surface wind divergence and convection over tropical oceans. *Science*, **238**, 657–659.
- Gregory, D. and P. Rowntree, 1990: A mass flux convection scheme with representation of cloud ensemble characteristics and stability-dependent closure. *Mon. Wea. Rev.*, **118**, 1483–1506.
- Held, I. M. and B. J. Soden, 2006: Robust responses of the hydrological cycle to global warming. *J. Climate*, **19**, 5686–5699.
- Hilburn, K. A. and F. J. Wentz, 2008: Intercalibrated passive microwave rain products from the unified microwave ocean retrieval algorithm (UMORA). *J. Appl. Meteor. Clim.*, **47**, 778–794.
- Holloway, C. E. and J. D. Neelin, 2007: The convective cold top and quasi equilibrium. *J. Atmos. Sci.*, **64**, 1467–1487.
- Holloway, C. E. and J. D. Neelin, 2008: Moisture vertical structure, column water vapor, and tropical deep convection. *J. Atmos. Sci.*, revised.
- Hu, Y. and R. T. Pierrehumbert, 2001: The advection-diffusion problem for stratospheric flow. Part I: Concentration probability distribution function. *J. Atmos. Sci.*, **58**, 1493–1510.
- Joseph, R. and S. Nigam, 2006: ENSO evolution and teleconnections in IPCC’s 20th century climate simulations: Realistic representation? *J. Climate*, **19**, 4360–4377.
- Kummerow, C., J. Simpson, O. Thiele, W. Barnes, A. T. C. Chang, E. Stocker, R. F. Adler, et al., 2000: The status of the Tropical Rainfall Measuring Mission (TRMM) after two years in orbit. *J. Appl. Meteorol.*, **39**, 1965–1982.
- Lin, J. W.-B. and J. D. Neelin, 2000: Influence of a stochastic moist convective parameterization on tropical climate variability. *Geophys. Res. Lett.*, **27**, 3691–3694.
- Lin, J. W.-B. and J. D. Neelin, 2003: Toward stochastic moist convective parameterization in general circulation models. *Geophys. Res. Lett.*, **30** (4), 1162, doi:10.1029/2002GL016203.
- Majda, A. J. and P. R. Kramer, 1999: Simplified models for turbulent diffusion: Theory, numerical modelling, and physical phenomena. *Phys. Rep.*, **314**, 237–574.
- Maloney, E. D. and D. L. Hartmann, 2001: The sensitivity of intraseasonal variability in the NCAR CCM3 to changes in convective parameterization. *J. Climate*, **14**, 2015–2034.
- Manabe, S., J. Smagorinsky, and R. F. Strickler, 1965: Simulated climatology of a general circulation model with a hydrological cycle. *Mon. Wea. Rev.*, **93**, 769–798.
- Manna, S. S., 1991: Two-state model of self-organized criticality. *Journal of Physics A Mathematical General*, **24**, L363–L369.
- Moorhi, S. and M. J. Suarez, 1992: Relaxed Arakawa-Schubert: A parameterization of moist convection for general circulation models. *Mon. Wea. Rev.*, **120**, 978–1002.
- Murphy, D. M. and T. Koop, 2005: Review of the vapour pressures of ice and supercooled water for atmospheric applications. *Q. J. R. Meteorol. Soc.*, **131**, 1539–1565, doi:10.1256/qj.04.94.
- Neale, R. B., J. H. Richter, and M. Jochum, 2008: The impact of convection on ENSO: From a delayed oscillator to a series of events. *J. Climate*, In press, doi:10.1175/2008JCLI2244.1.
- Neelin, J. D., C. Chou, and H. Su, 2003: Tropical drought regions in global warming and El Niño teleconnections. *Geophys. Res. Lett.*, **30** (24), 2275, doi:10.1029/2003GL018625.
- Neelin, J. D. and I. M. Held, 1987: Modelling tropical convergence based on the moist static energy budget. *Mon. Wea. Rev.*, **115**, 3–12.
- Neelin, J. D., O. Peters, J. W.-B. Lin, K. Hales, and C. E. Holloway, 2008: Rethinking convective quasi-equilibrium: observational constraints for stochastic convective schemes in climate models. *Phil. Trans. Royal Soc. A*, **366**, 25812604.
- Neelin, J. D. and N. Zeng, 2000: A quasi-equilibrium tropical circulation model—formulation. *J. Atmos. Sci.*, **57**, 1741–1766.
- Pan, D.-M. and D. A. Randall, 1998: A cumulus parameterization with a prognostic closure. *Quart. J. Roy. Meteor. Soc.*, **124**, 949–981.
- Parsons, D. B., K. Yoneyama, and J.-L. Redelsperger, 2000: The evolution of the tropical western Pacific atmosphere-ocean system following the arrival of a dry intrusion. *Quart. J. Roy. Meteor. Soc.*, **126**, 517–548.
- Peters, O. and J. D. Neelin, 2006: Critical phenomena in atmospheric precipitation. *Nature Physics*, **2**, 393–396, doi:10.1038/nphys314.
- Peters, O., J. D. Neelin, and S. W. Nesbitt, 2008: Mesoscale convective systems and critical clusters. *J. Atmos. Sci.*, revised.
- Pierrehumbert, R. T., 2000: Lattice models of advection-diffusion. *Chaos: An Interdisciplinary Journal of Nonlinear Science*, **10** (1), 61–74, doi:10.1063/1.166476.
- Plant, R. S. and G. C. Craig, 2008: A stochastic parameterization for deep convection based on equilibrium statistics. *J. Atmos. Sci.*, 87 V–105.
- Pumir, A., B. I. Shraiman, and E. D. Siggia, 1991: Exponential tails and random advection. *Phys. Rev. Lett.*, **66**, 2984–2987, doi:10.1103/PhysRevLett.66.2984.
- Ramage, C. S., 1977: Sea surface temperature and local weather. *Mon. Wea. Rev.*, **105**, 540–544.

- Randall, D., M. Khairoutdinov, A. Arakawa, and W. Grabowski, 2003: Breaking the cloud parameterization deadlock. *Bull. Amer. Meteor. Soc.*, **84**, 1547–1564.
- Randall, D. A. and D. M. Pan, 1993: Implementation of the Arakawa-Schubert cumulus parameterization with a prognostic closure. *The Representation of Cumulus Convection in Numerical Models of the Atmosphere*, K. A. Emanuel and D. J. Raymond, Eds., American Meteorological Society, Washington DC, Meteorological Monographs, Vol. 46, 137–144.
- Raymond, D. J., 2000: Thermodynamic control of tropical rainfall. *Quart. J. Roy. Meteor. Soc.*, **126**, 889–898.
- Raymond, D. J., C. Lopez-Carrillo, and L. L. Cavazos, 1998: Case-studies of developing east Pacific easterly waves. *Quart. J. Roy. Meteor. Soc.*, **124**, 2005–2034.
- Redelsperger, J.-L., D. B. Parsons, and F. Guichard, 2002: Recovery processes and factors limiting Cloud-Top height following the arrival of a dry intrusion observed during TOGA COARE. *J. Atmos. Sci.*, **59**, 2438–2457.
- Sherwood, S. C., 1999: Convective precursors and predictability in the tropical Western Pacific. *Mon. Wea. Rev.*, **127**, 2977–2991.
- Shraiman, B. I. and E. D. Siggia, 1994: Lagrangian path integrals and fluctuations in random flow. *Phys. Rev. E*, **49**, 2912–2927, doi:10.1103/PhysRevE.49.2912.
- Sobel, A. H., S. E. Yuter, C. S. Bretherton, and G. N. Kiladis, 2004: Large-scale meteorology and deep convection during TRMM KWAJEX. *Mon. Wea. Rev.*, **132**, 422–444.
- Spencer, R. W. and J. R. Christy, 1992: Precision and Radiosonde Validation of Satellite Gridpoint Temperature Anomalies. Part II: A Tropospheric Retrieval and Trends during 1979–90. *J. Climate*, **5**, 858–866.
- Tang, C. and P. Bak, 1988: Critical exponents and scaling relations for self-organized critical phenomena. *Phys. Rev. Lett.*, **60**, 2347–2350, doi:10.1103/PhysRevLett.60.2347.
- Tian, B., D. Waliser, E. Fetzer, B. Lambrigtsen, Y. Yung, and B. Wang, 2006: Vertical moist thermodynamic structure and spatialtemporal evolution of the MJO in AIRS observations. *J. Atmos. Sci.*, **63**, 2462–2485.
- Tompkins, A. M., 2001: Organization of tropical convection in low vertical wind shears: The role of water vapor. *J. Atmos. Sci.*, **58**, 529–545.
- Tompkins, A. M. and J. Berner, 2008: A stochastic convective approach to account for model uncertainty due to unresolved humidity variability. *J. Geophys. Res.*, in press.
- Tompkins, A. M. and G. C. Craig, 1998: Time-scales of adjustment to radiative-convective equilibrium in the tropical atmosphere. *Quart. J. Roy. Meteor. Soc.*, **124**, 2693–2713.
- Tost, H., P. Jöckel, and J. Lelieveld, 2006: Influence of different convection parameterisations in a GCM. *Atmos. Chem. Phys.*, **6**, 5475–5493.
- Trenberth, K. E., A. Dai, R. M. Rasmussen, and D. B. Parsons, 2003: The changing character of precipitation. *Bull. Amer. Meteorol. Soc.*, **84**, 1205–1217.
- Trenberth, K. E. and C. J. Guillemot, 1998: Evaluation of the atmospheric moisture and hydrological cycle in the NCEP/NCAR reanalysis. *Climate Dynamics*, **14**, 213–231.
- Trenberth, K. E. and J. G. Olsen, 1988: An evaluation and intercomparison of global analyses from the National Meteorological Center and the European Centre for Medium Range Weather Forecasts. *Bull. Amer. Meteorol. Soc.*, **69**, 1047–1057.
- Uppala, S. M. and coauthors, 2005: The ERA-40 re-analysis. *Quart. J. R. Meteorol. Soc.*, **131**, 2961–3012, doi:10.1256/qj.04.176.
- Webster, P. J., 1981: Mechanisms determining the atmospheric response to sea surface temperature anomalies. *J. Atmos. Sci.*, **38**, 554–571.
- Wei, D., A. Blyth, and D. Raymond, 1998: Buoyancy of convective clouds in TOGA COARE. *J. Atmos. Sci.*, **55**, 3381–3391.
- Wentz, F. J. and R. W. Spencer, 1998: SSM/I rain retrievals within a unified all-weather ocean algorithm. *J. Atmos. Sci.*, **56**, 1613–1627.
- Wilcox, E. M. and L. J. Donner, 2007: The frequency of extreme rain events in satellite rain-rate estimates and an atmospheric general circulation model. *J. Climate*, **20**, 53–69.
- Xu, K.-M. and K. A. Emanuel, 1989: Is the tropical atmosphere conditionally unstable? *Mon. Wea. Rev.*, **117**, 1471–1479.
- Xu, K.-M. and D. A. Randall, 1998: Influence of large-scale advective cooling and moistening effects on the quasi-equilibrium behavior of explicitly simulated cumulus ensembles. *J. Atmos. Sci.*, **55**, 896–909.
- Yano, J.-I., K. Fraedrich, and R. Blender, 2001: Tropical convective variability as $1/f$ noise. *J. Climate*, **14**, 3608–3616.
- Yano, J. I., W. W. Grabowski, G. L. Roff, and B. E. Mapes, 2000: Asymptotic approaches to convective quasi-equilibrium. *Quart. J. Roy. Meteor. Soc.*, **126**, 1861–1887.
- Yeomans, J., 1992: *Statistical Mechanics of Phase Transitions*. Oxford University Press.
- Yoneyama, K. and T. Fujitani, 1995: The behavior of dry westerly air associated with convection observed during the TOGA-COARE R/V Natushima cruise. *J. Meteor. Soc. Japan*, **73**, 2913–304.
- Yu, J.-Y., C. Chou, and J. D. Neelin, 1998: Estimating the gross moist stability of the tropical atmosphere. *J. Atmos. Sci.*, **55**, 1354–1372.
- Zhang, G. J. and N. A. McFarlane, 1995: Sensitivity of climate simulations to the parameterization of cumulus convection in the Canadian Climate Centre general circulation model. *Atmos.-Ocean*, **33**, 407–446.
- Zhang, G. J. and H. Wang, 2006: Toward mitigating the double ITCZ problem in NCAR CCSM3. *Geophys. Res. Lett.*, **33**, L06709, doi:10.1029/2005GL025229.